Direct Calculation of the Tube Potential Confining Entangled Polymers

Qiang Zhou and Ronald G. Larson*

Department of Mechanical Engineering, University of Michigan, Ann Arbor, Michigan 48109-2036

Received March 24, 2006; Revised Manuscript Received July 5, 2006

ABSTRACT: We directly compute, for the first time, a confining "tube" potential acting on a flexible or semiflexible polymer chain entangled with like chains using equilibrium molecular dynamics simulations and compare these results to the conventional tube diameter inferred from the plateau in the time-dependent relaxation modulus $G(t)$ and to an apparent tube diameter inferred from the crossover time τ_e from $t^{1/2}$ to $t^{1/4}$ scaling in the time-dependent monomer diffusivity $g_2(t)$. We find that the "narrow" tube diameter obtained at the equilibration time τ_e, where the monomer first "feels" that it is in a tube, widens with time as the tube potential softens and develops a nonquadratic tail. Our results help explain why the value of the entanglement spacing inferred by measurements at time scale τ_e is only half the conventional value obtained by measurements of the plateau modulus in the vicinity of the Rouse time τ_R.

I. Introduction

The molecular weight dependence of the zero-shear viscosity of linear polymer melts, $\eta_0(M)$, shows two distinctive regimes,[1] separated by a critical molecular weight, M_C. A linear regime, $\eta_0(M) \propto M$, is found at low molecular weights, $M < M_C$, where polymers behave as unentangled molecules in a viscous medium. In this regime, intermolecular interactions only serve to screen hydrodynamic interactions and chain expansion from intrachain excluded-volume interactions. The dynamics of polymer molecules in this regime are well described by the Rouse model.[2] A power law regime, $\eta_0(M) \propto M^{3.4}$, is found at high molecular weights, $M > M_C$, where intermolecular interactions impose persistent topological constraints on neighboring molecules. The dynamics in this regime are generally successfully predicted by the tube model of de Gennes and Doi and Edwards,[2,3] which assumes that motion of a high-molecular-weight polymer is confined to a tubelike region, along which it meanders in a motion called reptation.

Beyond the parameters needed to define the Rouse model, the tube theory introduces only one additional parameter, the entanglement molecular weight M_e or the number of monomers between entanglements $N_e = M_e/M_0$, where M_0 is the monomer molecular weight. M_e is usually 2−5 times smaller than M_C.[4] The tube theory assumes that N_e is uniquely specified, while experiments and simulations have given estimates that can vary by a factor of 2 depending on the definition used. Most commonly, N_e is estimated from the "plateau modulus" G_N^0 through the standard formula[2]

$$G_N^0 = \frac{4}{5}\frac{\rho k_B T}{N_e} \tag{1}$$

where ρ is the monomer number density, k_B is the Boltzmann constant, and T is the temperature. The plateau modulus is the value of the relaxation modulus over a time range for which the modulus is nearly time independent following a small step deformation. The value of N_e obtained from eq 1 has been confirmed by neutron spin-echo measurements of the relaxation of the dynamic structure factor for polyethylene over a time range similar to that over which the plateau modulus is measured.[5] Using the tube model, a different measure of entanglement, N_e', can be estimated from the equilibration time, τ_e, at which the average monomer diffusivity relative to the center of mass of the chain crosses over from a Rouse-like regime, $g_2(t) \propto t^{1/2}$, to an entanglement regime, $g_2(t) \propto t^{1/4}$, or yet another measure N_e'' is obtained from the longest Rouse time τ_R, which is the time at which $g_2(t)$ crosses over from $g_2(t) \propto t^{1/4}$ to $g_2(t) \propto t^{1/2}$. The value of N_e' obtained from τ_e was found to be $N_e' \approx 32$ in simulations of melts of flexible pearl necklace chains by Pütz et al.[6] However, for the same pearl necklace chains, this value of N_e' is about a factor of 2 smaller than N_e obtained using eq 1 in simulations of relaxation after step strains. Alternatively, yet another estimate, N_e^P, can be obtained from the average length of the primitive paths computed using a "cooling method" described by Everaers et al.[7] in which the ends of all pearl necklace chains are held fixed and beads along the same chain are allowed to overlap each other but not penetrate beads on other chains. As the temperature is decreased, the spring energy causes the chains to give up their internal slack and collapse onto the shortest paths that preserve the constraints of noncrossability with other chains. These shortest paths are considered to be the primitive paths, and their average length can be used to obtain N_e^P. In this way, Everaers et al.[7−9] validated eq 1 but with a $N_e^P \approx 65$ for the same flexible pearl necklace polymer chains discussed above, for which $N_e' = 32$. Finally, G_N^0 was calculated from a stress autocorrelation function in equilibrium molecular dynamics simulations by Sen et al.,[10] which gave a value of N_e, using formula 1, that was about half of N_e^P obtained by Everaers. However, the chains simulated by Sen et al. contained only 120 or fewer beads, which are too short to obtain a reliable stress plateau from which to obtain N_e. These differences in entanglement spacing are evidently due to different ways of defining what a "tube" is and the time scale over which it is defined. Since the value of the entanglement spacing is such an important parameter in rheological models of entangled polymers, it is important to obtain a thorough understanding of the relationship between its value and the measurement method used.

In this work, we study this problem using extensive equilibrium molecular dynamics simulations of semiflexible polymer chains with up to 8.7 entanglements each estimated using N_e^P obtained from a primitive path analysis. This polymer chain

10.1021/ma060670a CCC: $33.50
Published on Web 08/19/2006

length, $N = 200$, is roughly the longest length currently affordable in molecular dynamics (MD) simulations of the dynamics of entangled polymer melts out to their longest relaxation times. The rest of the paper is organized as follows: we describe the polymer model in section II, section III covers the shear relaxation modulus, section IV calculates N_e' and N_e'' through monomer diffusion studies, section V describes the confining potential of the tube, and we then summarize and conclude in section VI.

II. Polymer Model

In this work, polymers are represented by beads connected by short springs as in the model of Kremer and Grest.[11] Excluded-volume interactions are included through a repulsive Lennard-Jones potential:

$$U_{LJ}(r) = \begin{cases} 4\epsilon\left\{(\sigma/r)^{12} - (\sigma/r)^6 + \frac{1}{4}\right\}, & r \le r_c \\ 0, & r \ge r_c \end{cases}$$

where the cutoff distance $r_c = \sqrt{2}\sigma$ is chosen so that only the repulsive part of the Lennard-Jones potential is used. σ and $\tau_0 = (m\sigma^2/\epsilon)^{1/2}$ set the length and time scales, respectively, where m is the bead mass, $\epsilon = k_BT$.

A finitely extensible nonlinear elastic (FENE) potential is used here for the spring:

$$U_{FENE}(r) = \begin{cases} -0.5kR_0^2 \ln(1 - (r/R_0)^2), & r \le R_0 \\ \infty, & r \ge R_0 \end{cases}$$

The spring is made short and stiff enough so that there is not enough room between connected beads for another bead to pass between them. Thus, chain crossing is disallowed. We take the spring constant to be $k = 30\epsilon/\sigma^2$, and the maximum length of the spring to be $R_0 = 1.5\sigma$.[11]

In addition, a three-bead bending potential is applied:[12]

$$U_{bend}(r) = k_\theta(1 - \cos\theta)$$

where k_θ is the bending stiffness, and $\cos\theta_i = (\hat{\mathbf{r}}_i - \hat{\mathbf{r}}_{i-1})\cdot(\hat{\mathbf{r}}_{i+1} - \hat{\mathbf{r}}_i)$, with $(\hat{\mathbf{r}}_i - \hat{\mathbf{r}}_{i-1})$ the unit vector pointing from bead $i-1$ to bead i. In this work, we use $k_\theta = 2$, which leads to a semiflexible polymer with a packing length 0.36σ and a characteristic ratio (proportional to chain stiffness) of $C_\infty = 3.4$, while a standard flexible polymer, $k_\theta = 0$, has a packing length 0.68σ and $C_\infty = 1.75$. The packing length is defined as $p = (N-1)/(\rho\langle R^2\rangle)$, where $\langle R^2\rangle$ is the average end-to-end extension. Primitive path analyses yield values of $N_e^P = 65$ and 23 for the above flexible and semiflexible polymer melts, respectively.[7] The use of a semiflexible polymer chain therefore allows us to explore more densely entangled polymer melts than is possible with flexible ones at the same computational expense.

In our MD simulation, we integrate an equation of motion, namely

$$\ddot{\mathbf{r}}_i = -\nabla U - \Gamma\dot{\mathbf{r}}_i + \mathbf{W}_i(t) \qquad (2)$$

where $\mathbf{r}_i$ is the position vector for bead i, and the potential U is comprised of the pairwise Lennard-Jones potential, the FENE potential, and the three-body bending potential given above. The segment number density is here set at $\rho = 0.85\sigma^{-3}$. The average monomer length is $\langle l^2\rangle^{1/2} = 0.97\sigma$ and the statistical segment length $b = 1.83(5)\sigma$. In our study of monomer diffusion, we perform constant NVT simulations, where the periodic cubic simulation box is coupled with a thermostat through a random force term, $\mathbf{W}_i(t)$, and a dissipation term, $\Gamma\dot{\mathbf{r}}_i$. $\mathbf{W}_i$ is a Gaussian white noise, which is related to the friction coefficient, Γ, by $\langle\mathbf{W}_i(t)\cdot\mathbf{W}_j(t')\rangle = \delta_{ij}\delta(t-t')6k_BT\Gamma$. The temperature is kept at around $T = \epsilon/k_B$ during the simulations, and $\Gamma = 0.5m/\tau_0$. To obtain the shear relaxation modulus, we carry out constant NVE simulations in a microcanonical ensemble imposed by setting $\Gamma = 0$. The velocity-Verlet method is used in the integration with a time step size of $\Delta t = 0.01$ in constant NVT simulations, while $\Delta t = 0.005$ is used for constant NVE simulations in order to conserve total energy within 0.5% during the whole simulation.

Table 1. System Sizes Studied[a]

$M \times N$	100×25	50×50	100×100	120×200
Z^P	1.09	2.17	4.35	8.70
$\sqrt{\langle R^2\rangle}/L$	0.62	0.89	0.79	0.84
$T(\tau_0)$	3×10^5	5×10^5	7×10^5	1×10^6

[a] M is the number of chains, N is the number of beads per chain, Z^P is the number of entanglements per chain, estimated using $N_e^P = 23$, L is the side length of the simulation box, $\langle R^2\rangle$ is the average end-to-end extension of the chains, and T is the total simulation time performed in the equilibrium molecular dynamics simulation.

III. Shear Relaxation Modulus

The linear viscoelastic properties of entangled polymer melts are captured in the shear relaxation modulus, $G(t)$, which can be obtained by measuring shear stress as a function of time after a small step-shear is imposed on a sample: $G(t) = \sigma_{xy}(t)/\gamma_0$, where σ_{xy} is the shear stress and γ_0 is the step shear strain. Straightforward as it appears to be, $G(t)$ is very hard to obtain in this way in an MD simulation because it demands a very large polymer sample or large number of runs to obtain a statistically converged $G(t)$.

In equilibrium molecular dynamics simulation, however, $G(t)$ can be obtained instead through the stress autocorrelation function:

$$G(t) = (k_BT)^{-1}V\langle\sigma_{xy}(t+t_0)\sigma_{xy}(t_0)\rangle \qquad (3)$$

where V is the volume of the simulation box, and σ_{xy} is the shear stress defined as follows:

$$\sigma_{\alpha\beta} = \frac{1}{V}\left[-\sum_{i=1}^{MN} v_{\alpha i}v_{\beta i} + \frac{1}{2}\sum_{i,j=1}^{MN}\frac{r_{\alpha ij}r_{\beta ij}}{|r_{ij}|}\frac{dU_{ij}}{dr_{ij}}\right] \qquad (4)$$

where M is the number of chains and N is the number of beads per chain; $v_{\alpha i}$ is the α component of the velocity of bead i. r_{ij} is the connection vector pointing from the position of bead i to that of j, and $|r_{ij}|$ is the distance between bead i and bead j. U_{ij} is the overall potential involving both bead i and j. Four chain lengths are studied here, listed in Table 1: $N = 25$, 50, 100, and 200, with the number of entanglements per chain ranging from $Z^P = N/N_e^P = 1.09$ to 8.70, with N_e^P estimated using primitive path analysis. These polymer samples are prepared through the slow push-off method of Auhl et al.,[12] followed by a full MD simulation out to $5 \times 10^5\tau_0$. After this, an MD simulation is performed for a time up to $10^6\tau_0$ so that $G(t)$ is converged at large correlation times. The number of chains, M, is chosen so that the simulation box has a side length greater than the average end-to-end extension of the polymer chains.

A running average is performed, following Sen et al.,[10] between $0.9t$ and $1.1t$ for each value of t. Additionally, we averaged together the three equivalent components of the shear stresses, τ_{xy}, τ_{xz}, and τ_{yz}. Figure 1 shows the shear relaxation moduli for four different polymer chain lengths. All of the

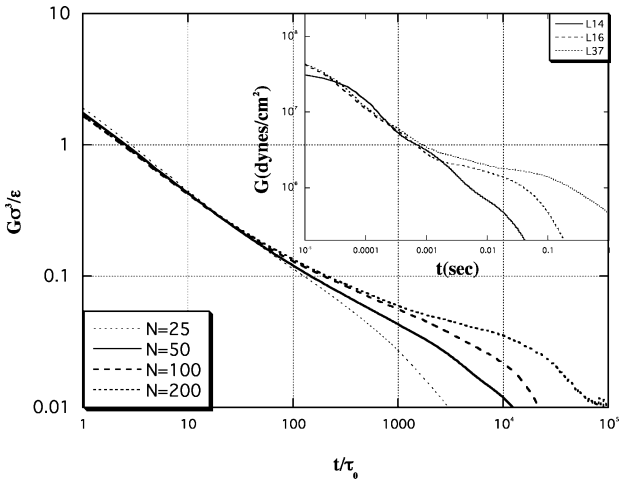

Figure 1. Shear relaxation moduli from equilibrium molecular dynamics simulations of semiflexible chains and from experimental data (inset) of Onogi et al.[13]

Table 2. Polystyrene Melts from Onogi et al.[13] [a]

	M_w	Z
L14	28 900	2.17
L16	58 700	4.41
L37	167 000	8.49

[a] M_w is the polystyrene molecular weight, and Z is the number of entanglements per chain, estimated using $M_e = 13\,309$.

moduli show a Rouse scaling regime, $t^{1/2}$, at early stages of the relaxation, $t < 100\tau_0$. As the chain length increases, the decay of $G(t)$ slows down dramatically at long times, which indicates a strong entanglement effect; however, even at a chain length of 8.70 entanglements, there is no clear-cut plateau in $G(t)$. Depending on what point along the $G(t)$ curve we take as the "plateau" modulus, the value of N_e will differ dramatically. For instance, $G(1800\tau_0) = 0.0523\epsilon\sigma^{-3}$ gives $N_e = 13$ using eq 1, while $G(18000\tau_0) = 0.0287\epsilon\sigma^{-3}$ yields $N_e = 26.7$. In Figure 1, we also compare our simulation results with data for experimental nearly monodisperse polystyrene melts with molecular weights 28 900, 58 700, and 167 000, corresponding respectively to 2.17, 4.41, and 8.49 entanglements with $M_e = 13\,309$ for polystyrene, which are listed in Table 2. Storage and loss moduli, G' and G'', are taken from Onogi et al.[13] To convert these to the time-dependent relaxation moduli $G(t)$, the data are then fitted by adjusting 10 sets of relaxation parameters g_i,τ_i using the simulated annealing method[14,15] to the following empirical formulas:

$$G'(\omega) = \sum_{i=1}^{10} g_i \frac{\omega^2\tau_i^2}{1+\omega^2\tau_i^2}$$

$$G''(\omega) = \sum_{i=1}^{10} g_i \frac{\omega\tau_i}{1+\omega^2\tau_i^2} \qquad (5)$$

$G(t)$ is then constructed from these sets of relaxation parameters using

$$G(t) = \sum_{i=1}^{10} g_i \exp(-t/\tau_i) \qquad (6)$$

The results, plotted in the inset of Figure 1, are qualitatively similar to our simulation results. A slowdown in the decay of $G(t)$ follows the initial Rouse relaxation, and no obvious plateau is found even at $Z = 8.49$. The chain lengths covered in these simulations are representative of those typically used in the MD studies of entangled polymer melts. Although the slowdown in the decay of $G(t)$ indicates a strong entanglement effect, these polymer lengths are not long enough to reveal a true plateau modulus, the appearance of which is an indication of a fully entangled polymer melt. As discussed in the following, the continuous decrease in $G(t)$ for this polymer chain length occurs in part because the polymer has not yet fully explored its tube as it relaxes.

IV. Monomer Diffusion

According to the tube theory, the mean-square monomer displacement relative to the center of mass of the chain, $g_2(t) = \langle(\mathbf{r}_{i,t} - \mathbf{R}_t - \mathbf{r}_{i,0} + \mathbf{R}_0)^2\rangle$, shows distinctive power laws for various time regimes. Using the notation of Pütz et al.,[6] these regimes are described by

$$g_2(t) = \begin{cases} 2b^2(Wt)^{1/2}, & t < \tau_e \\ \sqrt{\frac{2}{3}}\, bd_T(Wt)^{1/4}, & \tau_e \le t \le \tau_R \\ \sqrt{2}\, bd_T(Wt)^{1/2}/N^{1/2}, & \tau_R \le t \le \tau_d \\ R_G^2(N), & t \ge \tau_d \end{cases} \qquad (7)$$

where an average is taken over five center beads of the chain, $\mathbf{r}$ is the monomer position, $\mathbf{R}$ is the center of mass of the chain, $W = k_BT/\zeta b^2$, $d_T \propto \sqrt{R^2(N_e')}$ is the tube diameter, $R^2(N)$ is mean-square end-to-end separation of the ends of a chain composed of N monomers, ζ is the bead friction coefficient, b is the statistical segment length, τ_R is the Rouse time for relaxation along the primitive path, and τ_d is the disengagement or reptation time for the chain to escape the tube. From the tube model, we obtain $\tau_e = (N_e')^2/3\pi^2W$, $\tau_R = (Z')^2\tau_e$, and $\tau_d = 3Z'\tau_R$, where the number of entanglements per chain is $Z' = N/N_e'$ with N the number of monomers in the chain. The first transition from $g_2(t) \propto t^{1/2}$ to $g_2(t) \propto t^{1/4}$ reveals the existence of the tube, as shown by Kremer et al.[16] in MD simulations of flexible pearl necklace chains. The second transition from $g_2(t) \propto t^{1/4}$ back to $g_2(t) \propto t^{1/2}$ identifies the Rouse time and has not yet been shown in MD simulations. According to Pütz et al., flexible pearl necklace polymer chains of length $N = 350$ are too short to capture a clear second $g_2(t) \propto t^{1/2}$ regime before a third transition to $g_2(t) \propto t^0$ occurs at the crossover to reptative motion. However, if N_e'' were as low as 32 with $N = 350$, then the second regime $g_2(t) \propto t^{1/2}$ would theoretically extend for more than 3 decades and could be captured by calculations of $g_2(t)$.

Here we carry out simulations of semiflexible chain with two lengths, $N = 150$ and 300, which correspond to $Z'' \approx Z^p \equiv N/N_e^p = 6.5$ and 13 entanglements, respectively. Polymer samples were equilibrated using the slow push-off method of Auhl et al.,[12] followed by full MD relaxation for a time duration of $10^6\tau_0$. Internal configurations at all length scales were then checked against those of Auhl et al.[12] Thereafter, simulations were carried out for a time period of $2 \times 10^6\tau_0$ to study the diffusion process. Figure 2 shows the mean-square monomer displacement with respect to center of mass, $g_2(t)$, averaged over the center five beads. The first transition from $g_2(t) \propto t^{1/2}$ to $g_2(t) \propto t^{1/4}$ is clearly captured by both the short and long chains. Also captured by the short chain simulation (open circles) is the crossover to the

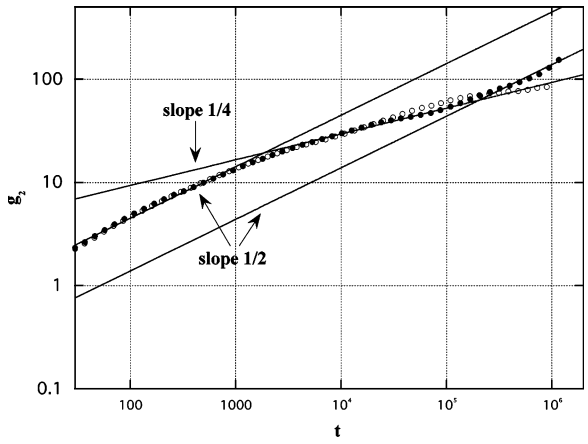

Figure 2. Mean-square monomer displacement relative to the center of mass of the semiflexible chain, $g_2(t)$, for chain lengths of 150 (○) and 300 (●).

free diffusion region, $t > \tau_d$, where $g_2(t)$ reaches a plateau. Prior to the plateau, a small upward deviation from $g_2(t) \propto t^{1/4}$ scaling also appears in the short-chain simulations. For the long chain (filled symbols), all three power-law regions are clearly captured, although the final crossover to the free-diffusion plateau is not reached in the time scale of the simulation. The first crossover point from $g_2(t) \propto t^{1/2}$ to $g_2(t) \propto t^{1/4}$ yields an estimate of $\tau_e = 1800 \pm 100\tau_0$ at the transition. The fitted line shown in Figure 2 for the first region is $g_2(t) = 0.447(5)\sigma^2(t/\tau_0)^{1/2}$. Following the procedure of Pütz et al., one gets $N'_e = 14 \pm 2$ using the value of τ_e obtained at the crossover point from this regime to the $t^{1/4}$ regime. However, from primitive paths identified by the cooling method, we obtain the estimate $N_e^P = 23 \pm 2$ for semiflexible chains of this packing length, which is consistent with the estimate obtained from G_N^0.[7] This plateau is reached after a small step strain, according to tube theory, at a time on the order of τ_R. From the second transition in $g_2(t)$ from $t^{1/4}$ to $t^{1/2}$, we estimate $\tau_R = (2.2 \pm 0.2) \times 10^5\tau_0$. Therefore, according to the tube theory, $Z'' = \sqrt{\tau_R/\tau_e} \approx 11$, which yields $N''_e = 27 \pm 2$, about twice as large as the value inferred from the first crossover time. This confirms that a polymer chain is exploring a more restricted region of space at the first crossover point (where $N'_e \approx 14$) than at the second, where $N''_e \approx 27$. The reasons for this, we believe, are twofold: first, a polymer is confined in a "soft" tube, in which at times in the vicinity of τ_e the chain continuously explores a larger and larger "tube" diameter rather than a fixed tube diameter as is assumed in the standard tube model. Second, the chain lengths that are currently studied are still not long enough to be well entangled. Short-chain-length effects, such as constraint release and primitive path fluctuations, can affect the polymer dynamics dramatically for short chains. We will explore these in detail in the following section.

V. Confining Potential of the Tube and Constraint Release

To determine the effective confining potential of the tube, we performed direct tube sampling (DTS) with standard flexible polymer chains of 350 monomers. Starting with an equilibrated polymer sample, MD simulations were performed with all the chain ends fixed, which quenches reptation motion and thermal constraint release as well as low-frequency Rouse motions and hence freezes the entanglement network. Polymer chains then only experience high-frequency Rouse motions by which each polymer chain samples the accessible configurations subject to the constraints that it does not cross the other chains or move its ends. We carried out one DTS simulation for a time of $1.5 \times 10^5\tau_0$ in a simulation box of 200 chains and then repeated the simulation with the same initial equilibrated polymer sample as a starting point but with a different seed for the random number generator. A total number of 30 repeat simulations were performed with the same starting configuration. During DTS, we collected the coordinates of all polymer chains after each time interval of $600\tau_0$ until 250 of time intervals were sampled for each simulation box. Therefore, for each N-bead chain, we constructed a sampled configuration space of $T_t = 250 \times 30 \times N$ bead coordinates.

Two cooling methods, energy minimization[7] and length minimization,[17] were used to identify the primitive paths with chain ends fixed for the same equilibrated initial configuration. One should be cautious about these primitive paths from the cooling methods in that they are but two of multiple methods[7,17−19] that have been suggested for computing "primitive paths", and the "true" or best method has not yet been identified. The width of the distribution of these primitive path lengths depends on how the system is cooled,[17] although, fortunately, the average lengths of these paths are almost identical for the two cooling methods used here. Furthermore, the paths are typically similar to each other and not far away from the centerline of the configuration space consisting of all possible configurations a polymer chain can take with ends of all chains fixed. Figure 3 shows a randomly selected primitive path from energy minimization (PPE, black line), and one from length minimization (PPL, white line), as well as the "cloud" of sampled chain configurations for a typical polymer chain. This "cloud" of sampling chains is quantified by sampling bead density as follows: The simulation box is first subdivided into $120 \times 120 \times 120$ equal-sized cells, and the sampled bead coordinates for each chain are assigned to the cells according to their locations. We then count the number of beads, n, in each cell and define the bead density for that cell as n/T_t. The resulting density isosurfaces, as plotted in Figure 3, represent the "confining tube". Note that the primitive paths, both PPE and PPL, are good approximations to the centerline of the confining tube, since they run roughly along the center of the tube defined by the isodensity surfaces. Figure 4 shows the correlation of PPE and PPL averaged over all chains in the simulation box, where $\mathbf{r}_E(s) = \mathbf{R}_E(s) - \mathbf{R}_E(0)$, $\mathbf{r}_L(s) = \mathbf{R}_L(s) - \mathbf{R}_L(0)$, and $\mathbf{R}_E(s)$ and $\mathbf{R}_L(s)$ are the PPE and PPL coordinates, respectively, at the curvilinear position s, which ranges from 0 at one end of the path to 1 at the other end. On average, these two primitive paths are closely correlated with each other although the widths of the distributions of primitive paths from the two methods are quite different.[17]

With the primitive paths identified for each simulation, we return to the uncooled system and measure the excursion, r, of a bead from this primitive path by finding the minimum distance of the bead from its corresponding position on the primitive path. For an end bead (bead 1), the corresponding position on the primitive path is identical to its own position since the end beads are frozen. For the next bead (bead 2), the point of projection is taken to be the point on the primitive path closest to bead 2, as long as this point of projection is "close" to the point of projection of the previous bead, bead 1 in this case. To define what is meant by "close", we note that the primitive path is given by the positions of the beads of the chain after they have been relocated by the cooling procedure. Our measure of "closeness" is that the projected location of the second bead must not be more than 20 beads distant from the projection of the first bead along the primitive path. (There is little sensitivity

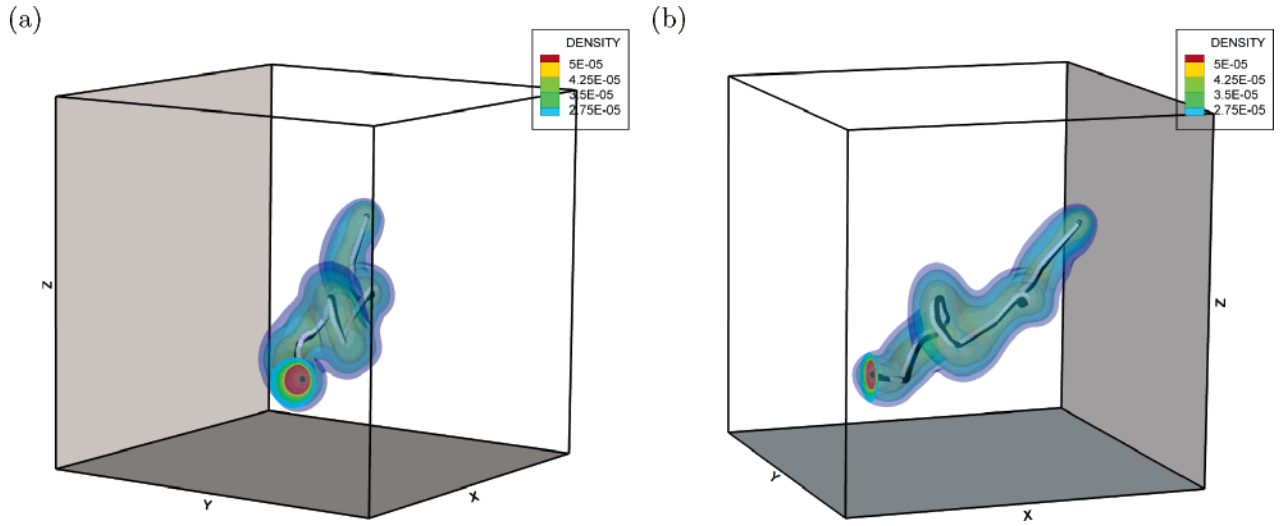

Figure 3. Direct visualization of a confining tube of a flexible chain. Black lines are primitive paths from energy minimization, and white lines are primitive paths from length minimization. The contour plots are isosurfaces of sampling bead densities.

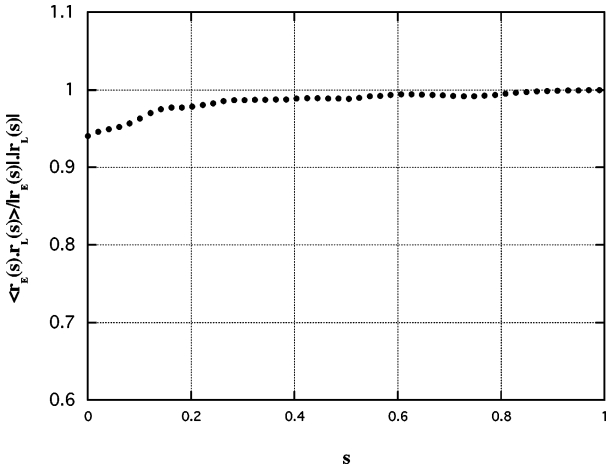

Figure 4. Correlation of primitive paths from energy minimization and length minimization as a function of contour length along the primitive paths of flexible chains.

to this choice for the measures of proximity ranging from 10 to 40 beads.) This exclusion is intended to reject projections onto distant parts of the primitive path that happen to be spatially close because of a loop in the primitive path contour. Continuing this process, we can find the projection of each bead to its closest position along the primitive path and the instantaneous distance of the excursion of that bead from its projected position.

The effective "radius" of a tube, r_T, is estimated by the excursion distance normal to the primitive path within which the beads are found a given percentage of the time. To minimize the end effects introduced by fixing the ends, only the internal 210 beads are considered when computing r_T. Figure 5 shows the evolution of the tube "radius" at four cutoff percentages: 60%, 70%, 80%, and 90%. The radii estimated from PPE coordinates are generally larger than those from PPL coordinates, indicating that the PPL is generally closer to the centerline of the confining tube. The radius at 90% bead probability is nearly twice as large as that at 60%, whose radius is very close to the radius predicted by Pütz et al. using their estimate of N_e' at time τ_e. Nonetheless, they all show a slow expansion of radius by about $9.5 \pm 0.9\%$ over a time period of $100\tau_e$, regardless of the cutoff percentage. Here $\tau_e = 1420$ is determined[6] from the transition point from the power law from $g_2(t) \propto t^{1/2}$ to $g_2(t) \propto t^{1/4}$, which gives $N_e' = 32$.

The probability density functions, at five different times, of finding a bead at a distance r/σ from the primitive path, $P(r/\sigma)$, are plotted in the inset of Figure 6. Since $P(r/\sigma)$ peaks at $r/\sigma = 0$, Figure 6 indicates that the primitive paths obtained from the cooling methods do represent, on average, the most likely configurations subject to the topological constraints. In addition, after freezing the end positions, the probability of finding a bead at a distance within r/σ of the primitive path progressively decreases as time increases. Larger excursions from the primitive path occur as DTS proceeds, indicating that the effective tube radius is increasing. The tube confining potential, $U(r/\sigma) = -k_BT \ln P(r/\sigma)$, is also shown in Figure 6. A quadratic potential is obtained at all times for excursions $r/\sigma \leq 5$, corresponding to a Gaussian distribution. At large excursions, however, the confining potential is nonquadratic and softens as time progresses. These features are not sensitive to the particular method used in finding the primitive paths, as seen by comparing Figure 6a with Figure 6b.

The softening of the potential arises in part from a new type of constraint release event, which differs from the constraint releases due to reptation and primitive path fluctuations, both of which require motion of chain ends. Although in our simulations chain ends are frozen, constraint release can still occur via "end looping" constraint release (ELCR) shown in Figure 7. A polymer chain (gray) can disentangle itself from a neighboring chain (black) by hopping an internal portion of itself over one end of the neighboring chain through Rouse motion. ELCR is expected to be relatively fast if a chain end is near the entanglement point but very rare if the chain end is distant. Nevertheless, given enough time, the central portion of a chain with fixed ends can form an extended hernia which might pass over a chain end, thus escaping an entanglement interaction or creating a new one. ELCR might be too slow relative to other constraint-release events in chains with free ends to be a significant relaxation mechanism in real melts. Still, this type of motion illustrates why no entanglement in a melt of chains with no rings is truly permanent, even when all chain ends are fixed. Only ring polymers are capable of forming mathematically rigorous topological "knots" with neighboring chains that permanently prevent chain crossing. For linear or branched polymers with no closed loops, entanglements are thus inherently time dependent, and the usefulness of the "tube" concept depends on the relative slowness of the increase of tube diameter due to constraint release processes relative to the rate of which

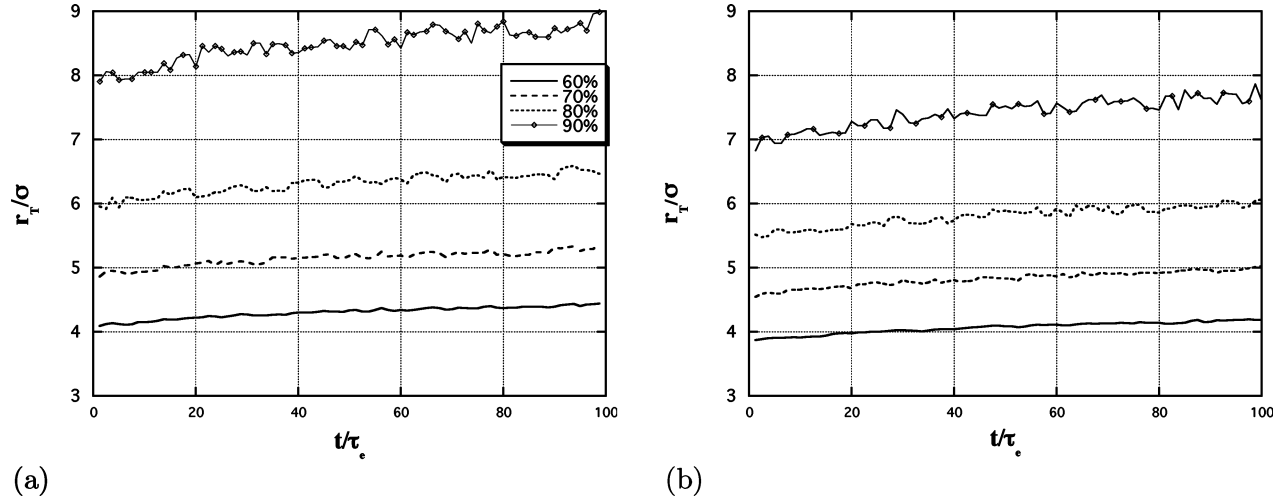

Figure 5. Evolution of tube radius of flexible chains. Primitive paths are obtained through minimizing (a) energy and (b) length.

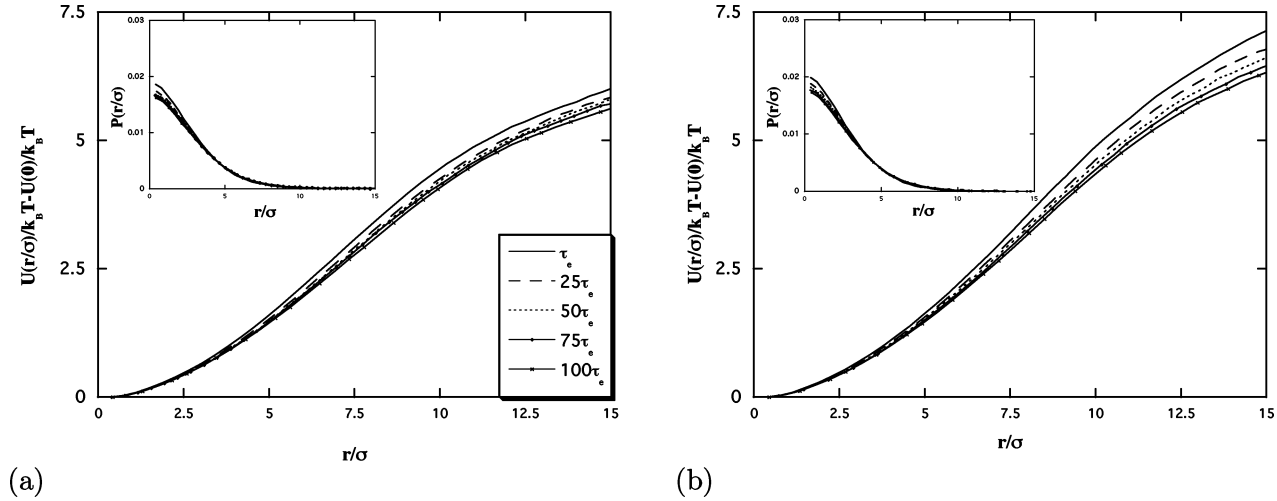

Figure 6. Tube confining potential of flexible chains at different times. Primitive paths are obtained through minimizing (a) energy and (b) length.

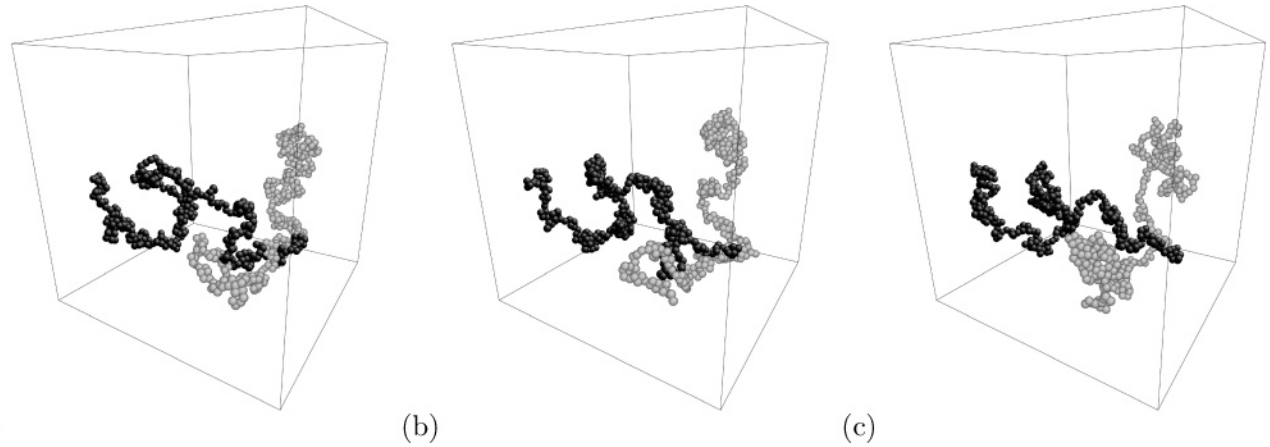

Figure 7. An end-looping constraint release event, plotted using AtomEye. The gray chain can hop over one end of the black chain during direct tube sampling, when chain ends are fixed.

the tube is escaped by reptation or primitive path fluctuations.

Constraint release by end looping is slowed by the relative unlikelihood of extended hernias that pass over chain ends. Such extended hernias are also important in "primitive path fluctuations", in which a chain end migrates deeply within a tube by extending out lateral unentangled hernias. End looping requires that these hernias be directed along an entangling chain so that they may pass over its end. The high unlikelihood of long, directed hernias is expected to produce a steep repulsive entropic potential that greatly slows down such motions after all shallow end-looping has occurred. Hence, for linear chains, end looping likely contributes significantly to tube widening only at relatively early times, if at all. For star polymers, or for more complex multiply branched polymers, end looping might contribute to constraint release even at long times, but this is yet to be demonstrated. We can estimate the entropic penalty for creating a hernia containing N_{loop} monomers that extends a contour distance s from an entanglement point as $S_{loop}/k_BT \approx N_{loop}/N_e$

$+ s^2/N_{loop}b^2$, where the first term is the entropy of sequestering N_{loop} monomers into an unentangled loop and the second term is the Gaussion entropy of stretching that loop around the other primitive path. Choosing the value of N_{loop} that minimizes this entropy yields $N_{loop} \approx N_e^{1/2}s/b$ and an entropy of $S_{loop}/k_BT \approx 2s/a = 2\xi Z$, where $a = N_e^{1/2}$ is the tube diameter and $\xi = s/Za$ is the fractional distance the loop must extend along the entangling chain's primitive path to reach the chain end. This linear potential exceeds the quadratic potential governing primitive path fluctuations for small distances ξ but becomes comparable to it for ξ near unity.

The soft tube-confining potential, further softened by end-looping constraint release, may help us understand several discrepancies between predictions of the original tube theory and results from simulations or experiments. N_e' found from τ_e at the crossover of $g_2(t)$ from $t^{1/2}$ to $t^{1/4}$ behavior is smaller (by a factor of 2) than the value $N_e'' \approx N_e^p$ obtained from the Rouse time because a polymer chain continues to explore larger distances from the primitive path as diffusion proceeds. This is probably also the reason for the broad and gradual transition from one power-law scaling to another in $g_2(t)$.

VI. Summary

In summary, we have calculated the confining tube potential, the monomer diffusivity, and the shear relaxation modulus, $G(t)$, in MD simulations of flexible and semiflexible polymer melts. A dramatic slowdown in the decay of $G(t)$ is found after the initial Rouse relaxation, which indicates a strong entanglement confinement effect in the dynamics of the polymer chains. However, no clear-cut plateau was found in $G(t)$ even for a chain of $Z^p = N/N_e^p = 8.7$ entanglements, consistent with experimental data for polystyrene melts with 8.49 entanglements per chain. This arises in part because polymer chains of these lengths effectively experience a dilating tube as the chain gradually explores larger and larger distances from the primitive path. Our MD simulations of semiflexible linear polymers also capture three power-law scaling regimes of monomer diffusion predicted by tube theory. In agreement with the results for $G(t)$, the monomer diffusivity indicates that the diameter of the effective confining tube expands with time, indicating that a single value for the monomer spacing between entanglements does not apply over the time range from τ_e to τ_R.

The expanding tube is the result of the soft confining potential and constraint release that, surprisingly, can occur even for fixed chain ends, which weakens the confining potential at longer times. A new constraint release mechanism, end looping, which does not require movement of chain ends, is also discovered in this work. In conclusion, our finding that the tube expands with time explains the discrepancy between the small values of N_e obtained from measurements of short-time relaxation phenomena, such as the early-time crossover of $g_2(t)$ at τ_e, and larger values of N_e obtained at times a which the plateau modulus is measured.

Acknowledgment. This work was supported by the NSF under Grant DMR 0305437 and supported by the National Computational Science Alliance under PHY040025N, utilizing the IBM P690 and the Xeon Linux Supercluster. Helpful discussions with Dr. Shanbhag and Mr. Heo are gratefully acknowledged.

References and Notes

(1) Berry, G. C.; Fox, T. G. The viscosity of polymers and their concentrated solutions. *Adv. Polym. Sci.* **1968**, *5*, 261−357.

(2) Doi, M.; Edwards, S. F. *The Theory of Polymer Dynamics;* Oxford University Press: New York, 1986.

(3) de Gennes, P. G. Reptation of a polymer chain in the presence of fixed obstacles. *J. Chem. Phys.* **1971**, *55*, 572−579.

(4) Fetters, L. J.; Lohse, D. J.; Milner, S. T.; Graessley, W. W. Packing length influence in linear polymer melts on the entanglement, critical, and reptation molecular weights. *Macromolecules* **1999**, *32*, 6847−6851.

(5) Schleger, P.; Farago, B.; Lartigue, C.; Kollmar, A.; Richter, D. Clear evidence of reptation in polyethylene from neutron spin echo spectroscopy. *Phys. Rev. Lett.* **1998**, *81*, 124−127.

(6) Putz, M.; Kremer, K.; Grest, G. S. What is the entanglement length in a polymer melt? *Europhys. Lett.* **2000**, *49*, 735−741.

(7) Everaers, R.; Sukumaran, S. K.; Grest, G. S.; Svaneborg, C.; Sivasubramanian, A.; Kremer, K. Rheology and microscopic topology of entangled polymeric liquids. *Science* **2004**, *303*, 823−826.

(8) Kremer, K.; Sukumaran, S. K.; Everaers, R.; Grest, G. S. Entangled polymer systems. *Comput. Phys. Commun.* **2005**, *169*, 75−81.

(9) Sukumaran, S. K.; Grest, G. S.; Kremer, K.; Everaers, R. Identifying the primitive path mesh in entangled polymer liquids. *J. Polym. Sci., Part B: Polym. Phys.* **2005**, *43*, 917−933.

(10) Sen, S.; Kumar, S. K.; Keblinski, P. Viscoelastic properties of polymer melts from equilibrium molecular dynamics simulations. *Macromolecules* **2005**, *38*, 650−653.

(11) Kremer, K.; Grest, G. S. Dynamics of entangled linear polymer melts − a molecular-dynamics simulation. *J. Chem. Phys.* **1990**, *92*, 5057−5086.

(12) Auhl, R.; Everaers, R.; Grest, G. S.; Kremer, K.; Plimpton, S. J. Equilibration of long chain polymer melts in computer simulations. *J. Chem. Phys.* **2003**, *119*, 12718−12728.

(13) Onogi, S.; Masuda, T.; Kitagawa, K. Rheological properties of anionic polystyrenes. i. dynamic viscoelasticity of narrow-distribution polystyrenes. *Macromolecules* **1970**, *3*, 109−116.

(14) Jensen, E. A. Determination of discrete relaxation spectra using Simulated annealing. *J. Non-Newton. Fluid Mech.* **2002**, *107*, 1−11.

(15) Goffe, W. L.; Ferrier, G. D.; Rogers, J. Global optimization of statistical functions with simulated annealing. *J. Econom.* **1994**, *60*, 65−99.

(16) Kremer, K.; Grest, G. S.; Carmesin, I. Crossover from rouse to reptation dynamics − a molecular-dynamics simulation. *Phys. Rev. Lett.* **1988**, *61*, 566−569.

(17) Zhou, Q.; Larson, R. G. Primitive path identification and statistics in molecular dynamics simulations of entangled polymer melts. *Macromolecules* **2005**, *38*, 5761−5765.

(18) Shanbhag, S.; Larson, R. G. Chain retraction potential in a fixed entanglement network. *Phys. Rev. Lett.* **2005**, 94.

(19) Kroger, M. Shortest multiple disconnected path for the analysis of entanglements in two- and three-dimensional polymeric systems. **2005**, *168*, 209−232.

MA060670A